

Marshall Plan Research Report

Shrinking Coastlines: Use of UAV LiDAR & SfM in the rocky intertidal

Author: Elizabeth Bushnell

SDSU MSc Candidate in GIScience
Department of Geography

Supervisors

FH-Prof. Mag. Dr. Gernot Paulus, MSc, MAS, Department of Geoinformation
and Environmental Technologies, Carinthia University of Applied Sciences,
Villach, Austria

Prof. Dr. Douglas (Doug) Stow, Department of Geography, San Diego State
University, San Diego, USA

Abstract

Climate change influences rocky intertidal environments from regional to global scales, with predictions of dramatic habitat loss resulting from sea level rise (SLR). The temporal and spatial limitations of traditional laboratory and field-based research methods may render them insufficient for studying SLR effects on rocky intertidal zones. Unoccupied Aerial Systems (UAS), LiDAR, small camera sensors, and Structure from Motion (SfM) photogrammetry offer new options that allow ecologists and geographers to study this ecosystem type from a novel perspective and scale. However, work remains in identifying and matching information needs with available remote sensing technologies and tools, as well as to conduct head-to-head comparisons of different methods to determine the best approach to mapping and monitoring rocky intertidal habitats. This research uses a stream bed in Villach, Austria as a proxy for the rocky intertidal environment and compares three-dimensional (3-D) topographical data products from UAS LiDAR and UAS SfM to quantify how well each captures surface detail, using rugosity as a metric. Results indicate that rugosity measurements derived from LiDAR and SfM data strongly agree with each other, likely with less noise than field measurements. DSMs generally agree with each other after correction of an unknown systematic vertical difference in the LiDAR datasets. Future work remains in exploring applicability of UAS remote sensing for mapping and monitoring of different habitats and in improving workflows for processing and analyzing 3-D point clouds.

Table of Contents:

Introduction	4
Purpose	6
Research Questions	6
Literature Review	6
1. Spatial Structuring of the Rocky Intertidal	7
2. Difficulties Studying Intertidal Climate Change	8
2.1 Laboratory Approaches	9
2.2 <i>In situ</i> Approaches	9
3. Remote Sensing as a Potential Solution for Difficulties Associated with In Situ Approaches	10
4. Possible Challenges of Remote Sensing in the Rocky Intertidal Environment	10
Methods	12
Study Areas and Associated Datasets	12
Data Collection	14
Data processing	16
Data Analysis	16
Results	18
Discussion & Conclusion	23
Future Work	25
Acknowledgements	25
References	26
Appendix: Agisoft Metashape Processing Report	30

Introduction

Understanding how species are organized into spatially structured communities is a key theme in ecology that overlaps with geography. Organization of species across environments is influenced by factors such as climate, body size, natural history, fecundity, and dispersal capability (Böhning-Gaese et al. 2006). Organization within environments depend on biotic and abiotic factors like competition, predation, temperature, substrate heterogeneity and habitat complexity (Connell, 1961; Camus et al. 1999; Carlson et al. 2006; Walker et al. 2009). The geography of the physical environment influences its ecological community structure.

Species richness and biodiversity increase with habitat complexity due to niche diversification (Dustan et al. 2013). Habitat complexity holds significant influence over the community structure of many environments. For example, habitat complexity influences size and abundance of organisms (Meager et al., 2011). Furthermore, substrate heterogeneity in the intertidal increases biodiversity (Camus et al., 1999). For example, the common periwinkle (*Littorina littorea*) is an herbaceous snail found in the rocky intertidal. Herbivores link upper and lower trophic levels, so their abundance and distribution has ramifications on producers and consumers in their ecosystem. Like most plants and animals, its distribution and abundance in the environment is not uniform. It has been found that while periwinkle distribution is variable across intertidal sites, density was positively correlated with rugosity (surface complexity) and the amount of exposed rocky substrate (Carlson et al. 2006).

Coral reefs are the classic example where benthic diversity is strongly influenced by reef rugosity and sea surface temperature (Mazzuco et al. 2020). Reef fish abundance and species richness increase with topographic complexity (Walker et al. 2009). Remote sensing has been used in benthic environments to estimate reef rugosity, but it does require specialized green wavelength bathymetric LiDAR (Brock et al. 2004) Measurements were performed along with *in situ* diver rugosity surveys, and LiDAR measurements from this study were found to reflect important benthic parameters, which is promising for the development of less intensive and invasive survey methods (Brock et al. 2004).

This pattern of habitat complexity and biodiversity cuts across benthic, intertidal, and terrestrial habitats. In the Pacific atoll of Tokelau, eight species of epigenic (non-burrowing) ant species coexist due to different utilization of habitat niches in accordance with their body size (Sarty et al. 2006). Rugosity can also affect partitioning of habitat among species adapted to move across different substrates (Collins et al. 2013). MacArthur & MacArthur (1961) demonstrated that bird diversity increases with environmental complexity

Much of ecology relies on field surveys. Rugosity is most often measured using the “chain and tape method”, in which a chain is gently draped over a profile of the substrate or feature of interest, and the ratio of the linear length of the profile and the surface length of the profile are taken, described further in Wallbridge et al. 2018. Other methods exist for estimating surface roughness, but the chain and tape method has been used since the 1970s to measure surface complexity of reefs (as well as other habitats) and is the most widely used method for doing so. Pais et al. (2013) analyzed the strengths and weaknesses of this method, noting that it cannot “distinguish among substrata with very different profiles, especially between a single large corrugation and a series of small corrugations.” Frost et al. (2005) compared complexity estimates between the chain and tape method, the use of profile gauges, and stereophotography in the rocky intertidal. They found that the results from the profile gauges and chain and tape method were similar, but stereophotography overestimated the complexity of smoother surfaces. Dustan et al. (2013) acknowledged that the chain and tape method lacks quantitative precision, and the chain can be invasive and potentially damaging to coral reefs. However, coral reefs are very environmentally sensitive. For other applications, it is useful for ground-based

estimation of habitat complexity, because it requires no specialized equipment, is straightforward enough to be done with minimal experience, it is not computationally intensive, and does not involve significant post-processing.

The difficulty with field-based surface roughness surveys is these efforts are environmentally invasive, labor- and time-intensive, and often have additional constraints, such as the tidal cycle in coastal environments, which limits the temporal- and spatial scales at which these surface roughness can be estimated (Garza, 2019). Coupled with rapid changes associated with climate change, these methods are insufficient; researchers need efficient means of data collection at more frequent and expansive scales (Garza, 2019). Remote sensing provides efficient, synoptic data collection that shows promise in ecology, particularly unoccupied aerial systems (UASs) for their low flying, high resolution capabilities. They offer quick mobilization, maneuverability, and inexpensive data collection relative to aircraft based remote sensing. LiDAR (light detection and ranging) and structure from motion (SfM) photogrammetry are two options that would likely be the most useful, as they can be used to create high resolution visual models of rocky intertidal sites, and capture the topography and three dimensional structure of the environment. Aircraft and satellite-based remote sensing yields data that are too coarse for this application, and are suited to environmental monitoring at coarser scales, such as for mapping forestry, agriculture, land use and land cover, or monitoring kelp forests (Nex and Remondino, 2013).

LiDAR and SfM photogrammetry are two remote sensing technologies commonly used with UAS for generating 3-D point clouds of surfaces. LiDAR works by emitting laser pulses that bounce off of the terrain below it, the backscatter is then collected by the sensor. The system has an onboard real-time kinematic (RTK) GPS that tracks its position with a high degree of precision. The elevation of these points are measured by how long it takes for the laser pulses to hit the terrain and bounce back to the sensor, producing a collection, or cloud of (x,y,z) points. SfM photogrammetry also produces a point cloud but does so by capturing images over the extent of the study area with substantial (e.g., 80%) forward and sideward overlap. Like LiDAR, UAS imaging systems used to capture images for SfM have an onboard global navigation satellite system (GNSS) for navigation and ideally, for triggering a camera (Loerch et al. (2022). Agisoft Metashape is an SfM photogrammetry software that uses artificial intelligence to identify match points in the image to estimate differential parallax and the interior and exterior orientation parameters of a set of overlapping aerial images. The (x,y,z) coordinates of the points are then triangulated using the relative displacement of the match points between images and the known location of the sensor. Studies of UAS-based LiDAR systems for surface roughness estimation are rare, because of the high cost of purchasing such systems. However, the cost of these systems is becoming more affordable from recent progress in the development of autonomous vehicles, pushing the development of LiDAR systems small enough to be compatible with drone systems (Lin et al., 2019).

Scientists are currently investigating whether aerial systems can yield images with an appropriate level of spatial detail to complement or replace traditional methods in the intertidal zone (Garza, 2019; Shaw et al 2019). Researchers have found that it can be difficult to achieve the same level of taxonomic resolution of organisms between *in situ* data and UAS SfM, but at a coarser level, the community composition in the two datasets was similar (Konar & Iken, 2017). Work remains to be done on the more immediate technical questions of identifying information needs as far as accurately mapping topography, substrate, and organisms at a fine level of detail. Furthermore, a thorough assessment of resolution, precision, and accuracy of UAS SfM as compared to UAS LiDAR is needed.

Purpose

The purpose of this research is to evaluate how accurately UAS-based LiDAR and Structure from Motion photogrammetry can estimate rocky surface texture in comparison to the established chain and tape field method. Secondly, the research provides a pilot study which informs my thesis research for the MSc in Geographic Information Science program at San Diego State University, an evaluation of the utility of UAS-based LiDAR and SfM in mapping and monitoring rocky intertidal habitats (RIH). I have the privilege to undertake this research in Villach, Austria at the Carinthia University of Applied Sciences (CUAS) as part of a summer exchange funded by the Marshall Plan Scholarship. Due to geographic constraints with the proximity of CUAS to RIH sites, my local supervisor at CUAS identified a nearby rocky stream bed which served as an analogous rocky land-water environment. Note that the original project title was kept for formal reasons, but this work may be more accurately described as a comparative assessment of UAS-LiDAR and -SfM in their capability to resolve detailed surface roughness

Research Questions

Given the context presented above, in this pilot study I addressed two research questions:

1. *How do spatial resolutions, horizontal and vertical accuracies, and densities of point clouds generated with UAS LiDAR and SfM photogrammetry compare?*
2. *To what extent do UAS LiDAR and SfM point cloud, DSMs, and orthoimage products accurately reflect ground truth/field-based measurements of rugosity (surface complexity or roughness) obtained using the traditional chain and tape method?*

Literature Review

The rocky intertidal zone is the coastal area between the fully marine environment just below low tide levels and the fully terrestrial splash zone above high tide (Underwood, 2000). This dynamic environmental gradient occurs over a few meters vertically, allowing for relative ease of observation (at limited spatial scales) (Underwood, 2000). Modern ecology owes much of its current understandings to the classical studies conducted in these environments (Connell, 1961; Paine 1966; Dayton 1971). Some have gone as far as saying the rocky intertidal is to ecology what fruit flies are to genetics (Garza, 2019). The physically intense environment, the steep environmental gradient, strong natural selection pressures create a fascinating environment to study; Tomanek & Helmuth poignantly refer to the rocky intertidal as a “natural laboratory” (2002).

Despite the immense research interest in this ecosystem, the rocky intertidal is understudied in the context of climate change and associated sea level rise. The rocky intertidal zone is subject to both terrestrial and oceanic climate changes phenomena and responds to climate change extraordinarily quickly compared to terrestrial environments. (Helmuth et al., 2006). In addition to sea level rise, other climate change effects, like increased temperature, and changes to upwelling regimes will also impact the community structure of rocky intertidal habitats as well as the biogeographic ranges of the organisms that live there (Helmuth et al. 2006). Thus, finding a way to efficiently map and monitor these rapidly changing environments is essential. Competitive pressure organizes intertidal species into distinct zonation bands (Connell, 1961; Dayton, 1971). These zonation bands are visible to some extent (Ellis, 2003). So, it is possible that remote sensing could be used to study changes to community structure over time at a relatively coarse species assemblage level. Using a combination of UAS-RGB and UAS-multispectral imagery, researchers have identified intertidal macroalgae species with 90% accuracy (Tait et al. 2019).

While climate change studies on salt marshes (Crosby et al., 2016) and mangroves (Cavanaugh et al., 2019) indicate that they are endangered by inundation, rocky intertidal habitats remain somewhat overlooked. Findings from extant literature consistently project dramatic changes, with over 50% of habitat lost in many cases (Jackson & McIlvenny 2011; Thorner et al. 2014; Kaplanis et al. 2020). Notably, rocky shores comprise about 80% of global coastlines (Jackson & McIlvenny, 2011). Much like mangroves and wetlands, rocky shorelines are typically also backed by urban development (or cliff faces) that would impede inland retreat of these environments with sea level rise, thus also subjecting them to the ‘coastal squeeze’, referring to the loss or deterioration of these coastal habitats as they are inundated under continued sea level rise. Research in Australia shows that spatial variability in the extent of lost habitat depends on local topography (Thorner et al., 2014). This is concerning as global mean sea level rise by 2100 is projected between 0.29 m and 1.10 m, dependent on carbon emission scenarios (Oppenheimer et al. 2019). This estimate may be too conservative, and an expected 1.8 m sea level rise by 2100 is also an estimate that is frequently used (Kaplanis et al. 2020). We may well exceed these (grim) expectations, as extreme scenarios predict as much as 2.5 m of sea level rise (Sweet et al. 2017). Given that sea level rise is not expected to be globally uniform (Thorner et al. 2014), the need for ecosystem- and region-specific research is vital.

Coastal environments are rapidly experiencing climate change impacts. The rocky intertidal zone is subject to both terrestrial and oceanic climate changes phenomena and responds to climate change extraordinarily quickly, displaying geographic range shifts as extreme as 50 km/decade (Helmuth et al., 2006). It is particularly difficult to study rocky intertidal habitats. Quadrat sampling is the most established method in ecology for studying these environments, but it is labor intensive, and limited in spatial and temporal extent at which it can be used (Garza, 2019). Discussion in the literature is limited, but the effects of spatial scale in marine habitats have not been sufficiently examined (Lecours et al., 2015). Following from this, quadrat sampling relies on an inherent assumption of geographic representation. Recent advancements in remote sensing technology make UAS-based intertidal research promising (Garza, 2019).

Through this review of the literature, I will address the following questions:

1. How do rocky intertidal ecosystems function and what is already known about how they respond to climate change?
2. What are the challenges and benefits with different approaches to studying these systems?
3. How has remote sensing been used to study these environments? What is the potential utility of UAS based remote sensing, particularly aerial imaging with structure from motion photogrammetry and aerial LiDAR?

1. Spatial Structuring of the Rocky Intertidal

Some of the early ecological research focused on rocky intertidal environments; the mechanics of these ecosystems, such as competition, tolerance, disturbance, predation, and biodiversity are well understood. Intertidal communities are intensely spatially organized, and characterized by distinct zonation bands. Generally, temperate intertidal habitats have a distinct upper mussel and barnacle zone, and a lower, more aquatic algal zone (Dayton, 1971). This is illustrated by Figure 1 (Davey, 2000).

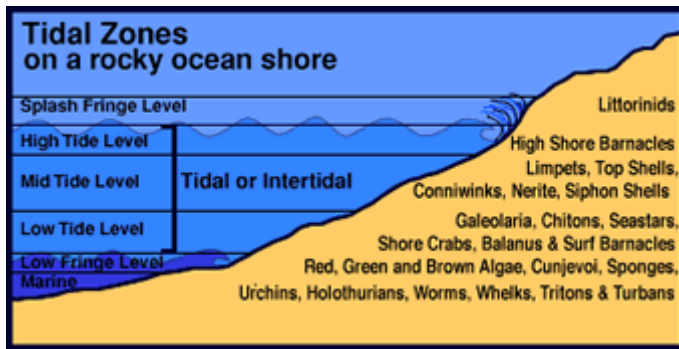


Figure 1 – Diagram of generalized intertidal zonation patterns, sourced from Davey, 2000.

Space is a limiting resource in the intertidal environment (Dayton 1971). Upper zonation limits are set by physiological tolerance, as there are limits to how much heat and desiccation the aquatic denizens of the rocky intertidal can withstand (Connell, 1961). Lower limits are set by biological interactions, such as predation and competition (Connell, 1961; Paine, 1966). Interspecific competition for space in rocky intertidal environments creates recognizable dominance patterns in which barnacles overgrow algae, and mussels overgrow both barnacles and algae (Dayton 1971). As Harley & Helmuth note, zonation patterns are heavily driven by the amount of time the rocky substrate is submerged by the tide, which is determined by the topography of the site (2003).

The intensity of spatial competition in this ecosystem raises the question: How is biodiversity maintained in an ecosystem where a foundational member can easily overtake other members? The answer lies in disturbance and predation. Drawing on a body of literature concerning biodiversity in various ecosystems, Connell (1961) proposed the Intermediate Disturbance Hypothesis (IDH) which posits that disturbances of intermediate frequency and severity maintain biodiversity by preventing the system from reaching equilibrium, thus preventing competitive exclusion or elimination of other species. The IDH is supported by both mixed terrestrial forests (often disturbed, but highly diverse) and staghorn corals (as of 1961, seldom disturbed and largely homogenous) (Connell, 1961). This explanation is so elegant and satisfying that it is still used by ecologists today; however, the seemingly implied assumption is that under the IDH, all competing species in an area are proportionately disturbed by these intermediate events, or they have inverse frequency dependent reproduction, such that a numerically common species cannot immediately overgrow its competitors following a disturbance.

Predation and mortality also play a role in preventing the ecosystem from reaching equilibrium, subsequently preventing the exclusion or elimination of species. So called “keystone predators” (notably sea stars) prevent the overgrowth of mussels (Paine, 1966). Physical variables such as heat, desiccation, wave exposure, and battering by drift logs also have important effects on abundances and distribution of sessile intertidal organisms and are a source of disturbance or mortality that provide space for colonization (Dayton, 1971). High mortality is a key characteristic of rocky intertidal habitats, with early post-settlement mortality in juvenile barnacles as high as 50% within the first 24 hours of settlement (Gosselin & Qian, 1996).

2. Difficulties Studying Intertidal Climate Change

Rocky intertidal community structure has been profoundly altered by climate change in comparison to historical data from the 1930s (Barry et al., 1995). How the rocky intertidal will respond to continued climate change is an area of active inquiry, with many interacting processes, and no small amount of uncertainty of future scenarios, largely hinging on actions by policy makers. However, given the community dynamics of the intertidal zone, and that the

organisms there have been evolutionarily optimized to colonize and compete for space, the expectation is that they will keep pace with sea level rise and shoreline retreat until they reach unsuitable substrate or further retreat is inhibited by a sea cliff or human structure (Harley et al., 2006). At that point, as the zonation “layer cake” is put under the coastal squeeze; many species will be outcompeted or unable to escape predation as the lower bounds move upward. Both laboratory-based and *in situ* studies of the rocky intertidal pose unique challenges.

2.1 Laboratory Approaches

Laboratory approaches to studying the rocky intertidal offer more controlled simulations of phenomenon of interest, as well as ease and frequency of observation, but are limited in relatability to the actual environment. Anticipated impacts of climate change in the intertidal include: increased temperature, increased sea surface temperature, decreased pH, increased stratification, a deeper thermocline, changes to upwelling, mismatches of reproduction, development, and resource availability due to phenological changes, decreased survivorship of calcifiers, secondary displacement of organisms that inhabit mussel beds, widespread biogeographic range shifts, as well as changes to habitat availability & zonation (Harley et al., 2006). Lab-based approaches can only focus on one or two key factors at a time (Findlay et al., 2009; Nasrolahi et al., 2016). Therefore, they lack a capacity to observe interactions between climate change effects. From an experimental design standpoint, it would be severely impractical, if not impossible to control and study interactions between that many variables. Several scholars have recognized this limitation and are calling for more holistic, integrated research on climate change (Harley et al., 2006; Helmuth et al., 2006; Mieszkowska et al., 2019; Kunze et al., 2021).

2.2 *In Situ* Approaches

In situ approaches avoid many of the shortcomings of laboratory approaches, but also face unique challenges. Traditionally, and still today, intertidal ecology relies on *in situ* surveys, transects, and quadrat sampling (Garza, 2019). These efforts are labor- and time-intensive, and need to be conducted at low-tide, limiting the temporal- and spatial scales at which researchers can study the intertidal (Garza, 2019). Coupled with rapid changes associated with climate change, these methods are insufficient; researchers need efficient means of data collection at more frequent and expansive scales (Garza, 2019).

Some intertidal literature used periodic temperature anomalies such as El Niño conditions, Pacific Decadal Oscillations, or warm ‘blob’ events as *in situ* proxies for climate change (Menge et al., 2008; Goddard et al., 2016). While these approaches creatively use unusual phenomena and are better contextualized to the real environment than lab studies, much like lab studies, they place particular emphasis on a single factor (temperature). Furthermore, relying on unusual conditions to study climate change could potentially introduce unintended confounding effects. Studies using El Niño conditions or other anomaly events as an approximation of anticipated climate change conditions may not accurately predict potential outcomes of climate change in coastal marine systems, as predictions of cold water species displacement by warm water species are rooted in broad correlations between seawater temperature and species abundance, and are not supported by longer studies on temperature increase from power plant outfall; it seems possible that some of these observations could be a product of anomalous conditions (Schiel et al., 2004).

The limited capacity of conducting field studies beyond small spatial extents carries the inherent major assumption that random quadrats are representative. Theoretically, a sufficiently large number of quadrats placed in a random, stratified manner to account for zonation should be statistically representative. However, the entire terrestrial to marine gradient occurs over a short distance vertically. (Underwood, 2000) and exhibits small-scale variability (Konar & Iken,

2017). Additionally, habitat complexity influences size and abundance of intertidal organisms (Meager et al., 2011). Furthermore, substrate heterogeneity in the intertidal increases biodiversity (Camus et al., 1999). Following from this, it seems that quadrat sampling is subject to the Modifiable Area Unit Problem (MAUP). The MAUP addresses the flawed assumption that relationships observed at one scale hold true at another, arising from the imposition of artificial spatial units on continuous geographic phenomenon, or combining data across different scales or levels of aggregation, thus generating artificial spatial relationships (Lecours et al., 2015). Thematic scales in ecology are sensitive to the MAUP, but the role of spatial scale in marine habitats lacks assessment necessary to determine what scale is fine enough (Lecours et al., 2015).

The MAUP is part of geographic theory, but it is known in ecology, albeit by a different name: the ecological fallacy. The idea of the ecological fallacy can be simply paraphrased as the erroneous idea that conclusions about individuals can be deduced from aggregate data of a larger group. Previously, ecologists gleaned information from spatially limited data as a result of constraints imposed by the environment. The role of spatial scale in intertidal ecology, and marine ecology in general is critically understudied, because scientists have lacked tools to study it. Given this issue, the ability to collect high spatial resolution, synoptic data, such as with remote sensing, could present a reliable solution.

3. Remote Sensing as a Potential Solution for Difficulties Associated with *In Situ* Approaches

Remote sensing is the process of collecting data about the physical environment without direct contact with the phenomena or areas of interest. Platforms for remote sensing range from satellites to drones and have been used to study inaccessible or dangerous areas, such as volcanoes (Kolzenburg et al., 2016) as well as sensitive environments, including mangroves, wetlands, kelp forests, and coral reefs, where minimal disturbance is preferable (Burns et al., 2015; Wang et al., 2019; Zhu et al., 2019; Doughty et al., 2021). Garza (2019) championed remote sensing as an option for intertidal field work, particularly with the advent of widely available, consumer-grade digital cameras and aerial drones.

LiDAR and structure from motion (SfM) photogrammetry are two remote sensing technologies for generating 3-D point clouds of surfaces. Point clouds can be processed to produce representations of 3-D surfaces. Digital cameras enable capturing detailed images of surfaces. When these sensors are on UAS, they enable high spatial resolution rendering of topography and surface features. UQS are mobile and enable some degree of spatial coverage of imagery to be captured. Digital cameras on low-flying piloted aircraft enable production of point clouds, DSMs, 3-D visualizations and orthoimage mosaics for more extensive areas at a lower spatial resolution. LiDAR can also be flown on these autonomous aircraft, but this approach is more expensive and requires more sophisticated technology and fairly extensive training.

4. Possible Challenges of Remote Sensing in the Rocky Intertidal Environment

Working with remote sensing involves matching available technology to information requirements. In the inherent nature of observations from a distance, remote sensing has an embedded tradeoff between coverage and resolution. Aircraft LiDAR in particular, is known to have up to 60 cm of vertical uncertainty, which may be limiting in the context of SLR, where cm differences in surface roughness may be significant (Enwright et al., 2018). However, UAS LiDAR or SfM allows data acquisition at a much closer distance to target than aircraft LiDAR.

SfM photogrammetry uses overlapping images and open-source software (e.g., Agisoft Metashape) to create 3-D point clouds and orthoimagery (Burns et al., 2015). While it is less expensive than LiDAR, and it features a largely automated workflow (Burns et al., 2015);

further work is necessary to assess the accuracy and precision of SfM- and LiDAR-derived point clouds, digital surface models (DSM) and orthomosaics. Kolzenburg et al. (2016) conducted such a comparison by integrating ground based SfM data with an existing aircraft LiDAR DEM and found that they could not effectively compare LiDAR & SfM in this case, because the spatial resolution of the SfM DEM was higher than the intrinsic error for the LiDAR dataset. However, one should consider the difference in scale between ground-based and aircraft datasets.

Methods

Study Areas and Associated Data Sets

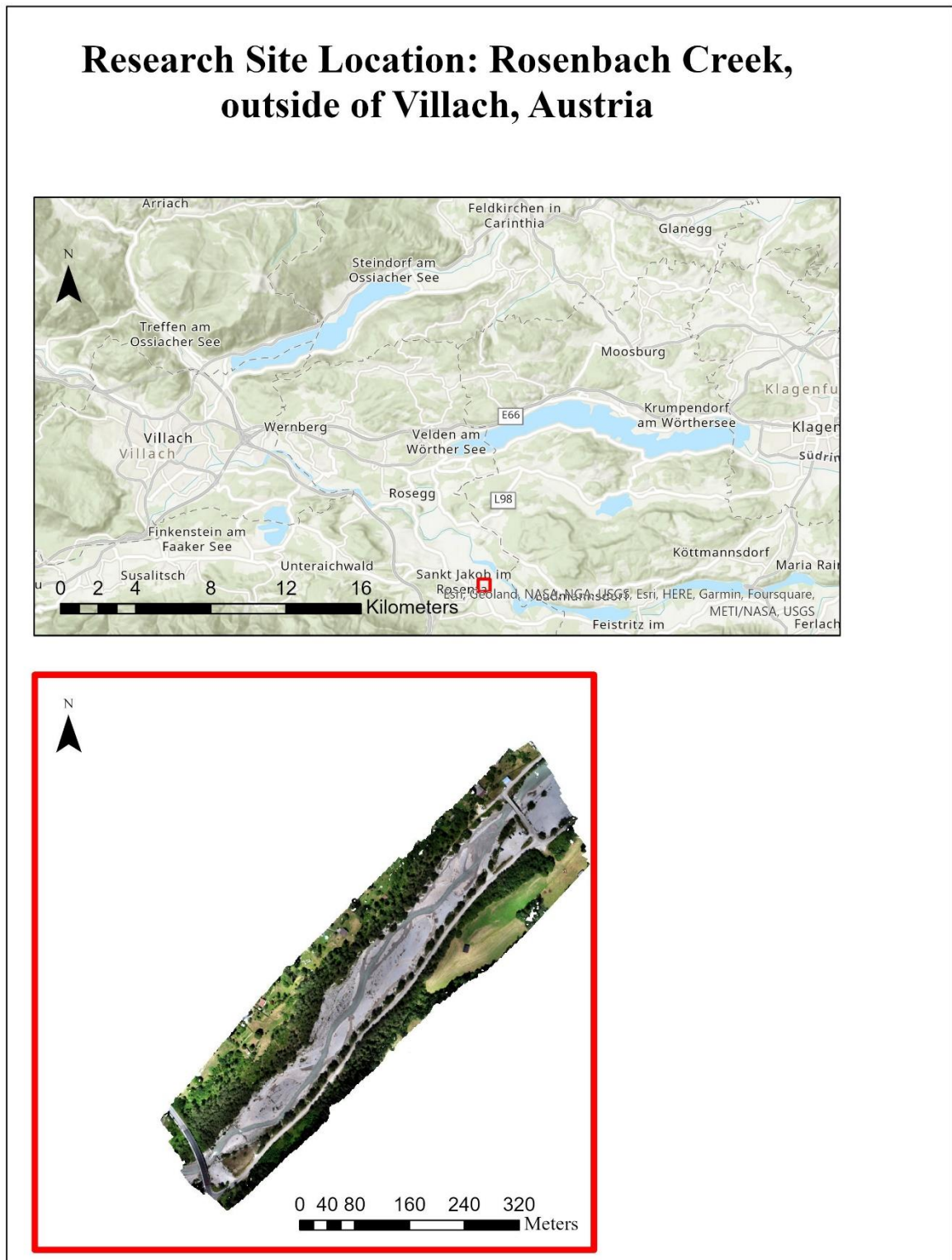


Figure 2 – A map showing the location of Rosenbach Creek outside of Villach, Austria, with the red square highlighting the study area. The smaller inset shows the orthoimage constructed from the site, and the distribution of GNSS points throughout the site.

An initial test was performed at Rosenbach Creek to demonstrate proof of concept that remote sensing can be used to complement field methods in ecology. Rosenbach Creek is located to the southeast of Villach, in south central Austria, near the border with Slovenia and Italy (Figure 2). The site is a highly urbanized riparian area, comprised mostly of flat, stony area. Larger rocky platforms as well as a road, vegetation and houses lie along the banks. UAS SfM photogrammetric and LiDAR datasets were collected, covering an area of 0.15 km². Ground reference data were also generated along 12 transects within a 5 m x 5 m subplot. The research area includes the creek, the surrounding banks and some areas with boulders. The subplot was in a mostly flat area, strewn with small rocks giving it subtle texture, which we used to see if the UAS systems could detect a fine level of detail. Figure 3 displays the locations of the transects, and a general schematic of the research design. Figure 4 shows the UAS flight plan for collecting the LiDAR data. Figure 5 is a ground photo at the study site, showing the area where measurements for the rugosity transects were recorded.

Field Sampling Plot Shown with DGPS Reference Points and Research Design Diagram

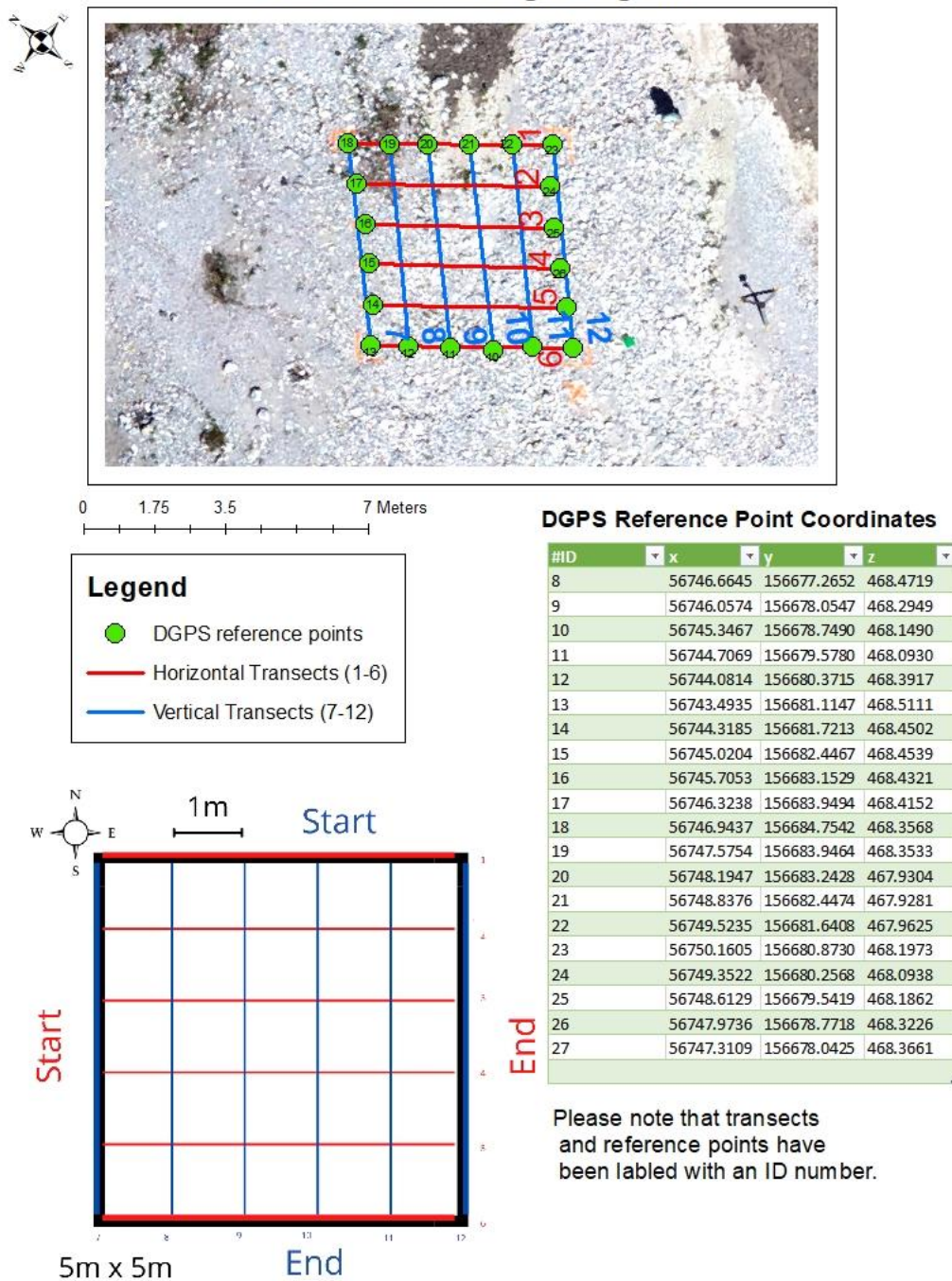


Figure 3 – Map of subplot transects, diagram of transect research design, survey grade GCPs (points 1 -7), and transect start and endpoints (points 8 – 27).

Data Collection

Data was collected from Rosenbach Creek on July 11, 2022 using UAS SfM, UAS LiDAR, and the previously mentioned field-based chain and tape method. Photogrammetric data was collected using a Phantom four RTK drone with a 20-megapixel FC6310R camera (focal length of 8.8 mm) at an altitude of 50 m. The positioning accuracy (RMS) for the Phantom four RTK is 1.5 cm + 1 ppm (vertical) and 1 cm + 1 ppm (horizontal). The drone collected 528 photos. UAS LiDAR data collection was done using a DGI M300 RTK drone at 70 m altitude equipped

with Zenmuse L1 Lidar sensor, with a ranging accuracy of 3 cm at 100 m ($\text{RMS } 1\sigma$)². The onboard RTK system has an accuracy of one cm + 1 ppm (horizontal) and 1.5 cm + 1 ppm (vertical). LiDAR data were collected with 40% overlap. Figure 4 shows the details of the LiDAR flight plan. There is no figure available for the SfM flight plan, but both missions covered the same area. All equipment specification information was taken from the DGI website.

Research collaborators collected ground reference data at Rosenbach Creek. They marked a 5 m by 5 m subplot, and six north-south and six east-west transects spaced 1 m apart. They marked the corners with square checkered plates, and the start and end points of the transects with orange spray paint. These points were also recorded using DGPS (Figure 3). Researchers then gently laid a chain along the substrate in a straight line and recorded the length of chain required to drape the surface profile. For a visual explanation of the chain and tape method, please refer to Figure 3 of Wallbridge et al. 2018. Researchers also recorded x,y,z coordinates around the perimeter of the subplot in 1 m increments, and seven survey-grade ground control points distributed around the research site (27 points total).

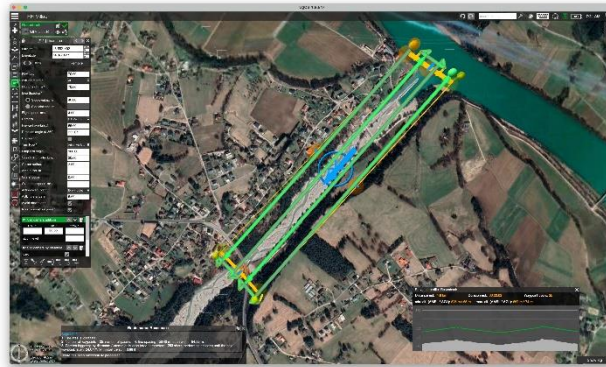


Figure 4 - The flight plan used to collect LiDAR imagery of Rosenbach Creek, covering an area of 0.15 km².



Figure 5 Ground photo of the study subplot where the rugosity transects were measured.

Data Processing: Structure from Motion

Digital frame images from the SfM-based mission were loaded into Agisoft Metashape and used to produce a dense (x, y, z) point cloud, orthoimage, and digital surface model (DSM). The point cloud had an average density of 0.15 points per cm². The resulting DSM and orthoimage had a resolution of 2.58 cm/pixel. The processing report is available in the appendix.

The DSM and orthoimage were then exported to ArcMap 10.6. The subplot was manually digitized, and Euclidean distances for the transects were measured digitally by snapping line segments between the recorded GNSS points at the start and end of each transect. The surface distances were measured from the DSM with the 3-D Analyst toolbox using the functional surface tool. Rugosity was calculated by dividing the surface measurement by the Euclidean measurement. the 3-D analyst tool was also used to investigate whether plot size impacted 2-D measurements of rugosity (surface area: planar area) within the visually homogeneous subplot.

Data Processing: LiDAR

The point cloud from the LiDAR mission was processed using TerraSolid. First, the XY coordinate system was changed from EPSG 31258 to EPSG 31255 to match the coordinate systems of the SfM dataset and the GCPs and then imported to Cloud Compare. After repeated attempts to rasterize the LiDAR dataset in Cloud Compare, I ultimately imported the LiDAR dataset into Agisoft Metashape and built a DSM using Agisoft Metashape's recommended cell size and extent settings (Figure 6). The DSM was then used in ArcMap with the 3D analyst tool to measure surface distance and calculate rugosity

Analysis Methods: DSM Comparison

To compare the two DSMs, the SfM DSM was re-exported from Agisoft Metashape to match the cell size and extent of the LiDAR DSM. Both DSMs were brought into Arc GIS Pro, and the SfM DSM was subtracted from the LiDAR DSM. At this point, there was an apparent upward shift of approximately four to five m in the LiDAR data, suggesting that the datasets were likely in different coordinate systems, but the vertical coordinate system was unknown. The SfM data was consistent with the GCPs, so it is assumed that there is an unknown source of error in the z dimension in the LiDAR dataset.

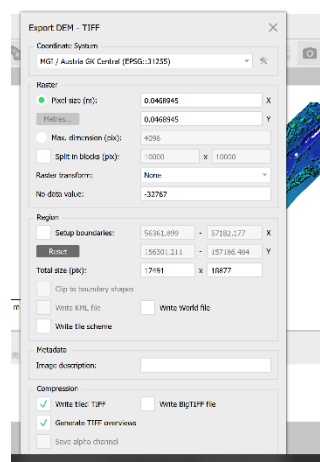


Figure 6– The Agisoft Metashape settings used to rasterize LiDAR data into a DSM.

After trying various likely candidates, no suitable vertical coordinate system was found, and ultimately it was determined that the best course of action was to come up with an average difference and apply a vertical bias correction to the LiDAR DSM. To do this, the distance between the LiDAR point cloud and each of the seven survey grade GCPs was measured and averaged, the result was then used to shift the LiDAR DSM down (Table 2).

Table 2 – The average distance between LiDAR point cloud and survey grade GCPs, used to apply a systemic correction to the LiDAR DSM.

GCP	X	Y	Z	Raster Value	Distance (m)
1	56742.28	156668.3	468.56	473.34	4.78
2	56706.45	156634.6	469.01	473.83	4.81
3	56649.28	156546.1	470.06	474.63	4.57
4	56642.06	156574.3	470.23	474.68	4.45
5	56673.69	156618.1	469.80	474.51	4.70
6	56694.64	156659.8	468.93	473.73	4.81
7	56753.97	156750.6	467.43	472.22	4.79
AVG					4.70
STDEV					0.138

Analysis Methods: Point Cloud Comparison

Creating DSMs from a 3-D point cloud requires spatial interpolation. It is worthwhile to compare 3-D data at the point cloud level as that is the primitive data stemming from LiDAR and SfM approaches. Given that the context of this research is to map and monitor rocky intertidal habitats, which are structured by tidal zonation and thus characterized heavily by elevation and geomorphic profiles, a comparison of how well the point clouds from the two approaches agree along the z axis is of interest. Further, recent work shows that the z axis for these types of datasets tends to have the most noise (Shaw et al. 2019; Elkrachy 2021).

I am currently developing a computer program to align two point clouds and subtract them with a nearest neighbor approach in Cloud Compare. To achieve this, and in an attempt to create an easier, more automated process for my thesis, which would involve doing this for multiple study sites, I am in the process of coding a python script that would read in two CSV files with (x, y, z) points, iterate through the smaller list, and find the nearest neighbor in the other list, implementing a KD tree data structure for spatial partitioning. The program will then generate a list of 2-D points comprised of the Z coordinates of the neighbor pairs such that $(x, y) = (Z_{SfM}, Z_{LiDAR})$. It will plot these points, perform a linear regression, visualize and output the results as a .png file. I expect to have the script done before mid-December, as I am attempting this as one of my class projects for the Fall 2022 semester at SDSU.

The linear regression approach described above will quantify the agreement between the two datasets and provide indications of systemic and random errors. The best-fit line will represent systemic bias, while the R^2 value would indicate random error. One potential source of random error is wind noise. Shaw et al. (2019) identified and accounted for random error in their research by plotting their data against a Weibull distribution. This approach could be taken if the R^2 value indicates a significant amount of random error in the datasets. Nafidi et al. (2019) examined Weibull distributions in depth and notes that they are “considered a useful model for survival populations, reliability studies, and life-testing experiments” but they are also often used to model wind speeds. While the reasoning behind the choice was not explained or justified in Shaw et al, this is most likely why the Weibull curve was used.

Results

SfM DSM Datasets

After the UAS images were aligned and optimized, the SfM point cloud had 316,838,818 points. During processing, the seven survey grade GCPs were used as control points and the four corners of the subplot were used as check points (Figure 7 & 8). The XY RMSE for the control points was 0.605 cm and the Z RMSE was 0.626 cm for a total of 0.871 cm. The total pixel error was 0.691 pix. The XY RMSE for the check points was 1.217 cm and the Z RMSE was 2.059 cm for a total of 2.392 cm. The total pixel error was 0.966 pix (Agisoft Metashape Processing Report).

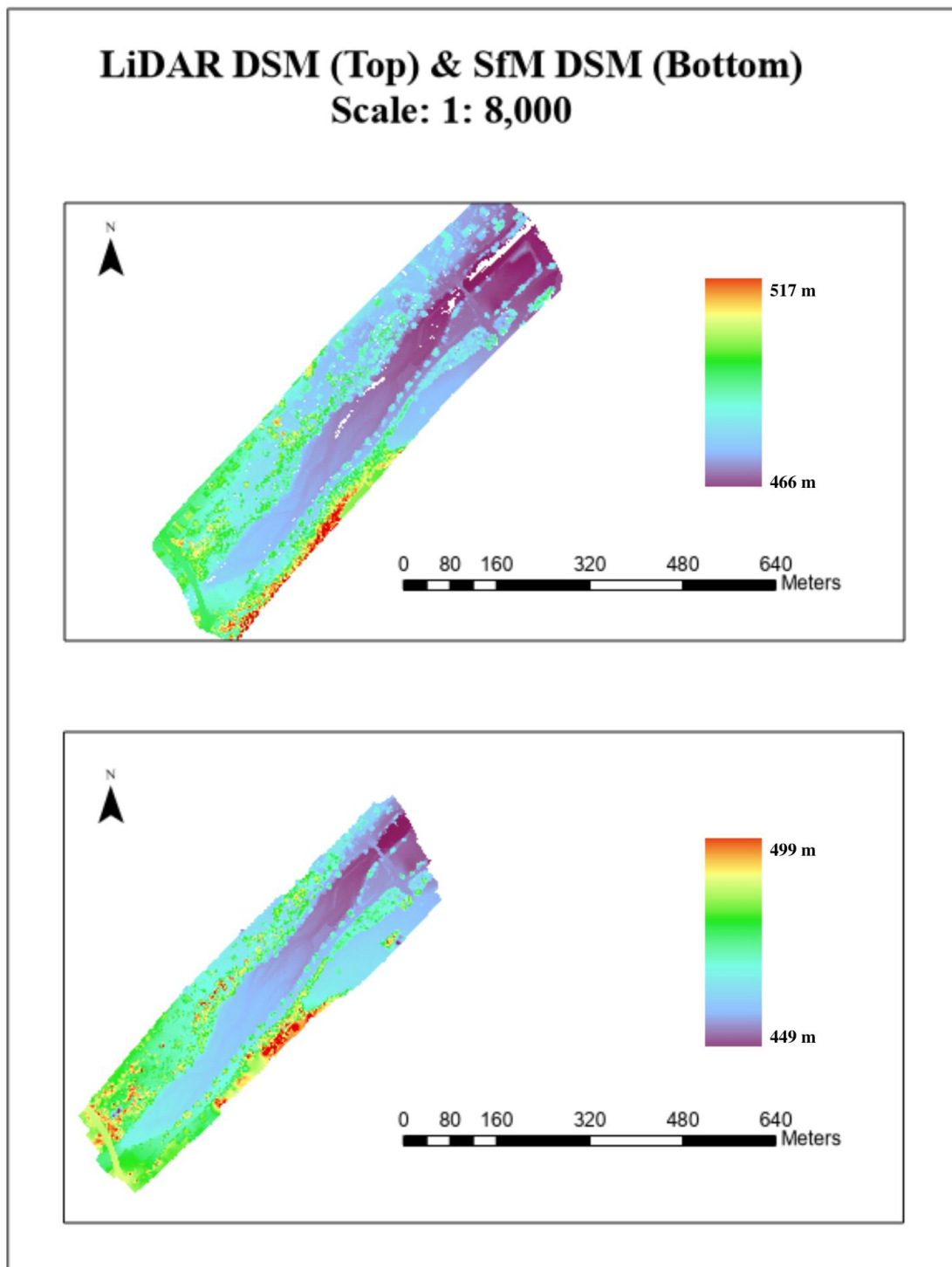


Figure 7 – The LiDAR and SfM DSMs shown side by side. Disagreement occurred mostly in vegetated areas due to differences in the two technologies and was expected.



Figure 8 – The SfM orthoimage with control points and check points shown.

The LiDAR point cloud contains 127,636,247 points, approximately one-third of the number of points in the SfM dataset. The pixel size of the LiDAR DSM is 4.7 cm (Figure 6). Interestingly, the vegetation (red areas toward the bottom right edge) registers at a higher elevation than the large bridge and roadway structures at either end. However, there are hillslopes and rocky platforms along either side of the creek at the edges of the DSM, so it does not seem inaccurate.

Visually, the SfM dataset is higher resolution than the LiDAR dataset, consistent with its higher point density (Figure 9). The SfM dataset provides a degree of detail visually similar to the orthoimage and landscape features are more visible in shaded areas as compared to the orthoimage. The LiDAR dataset is a bit coarser with a patchy appearance.

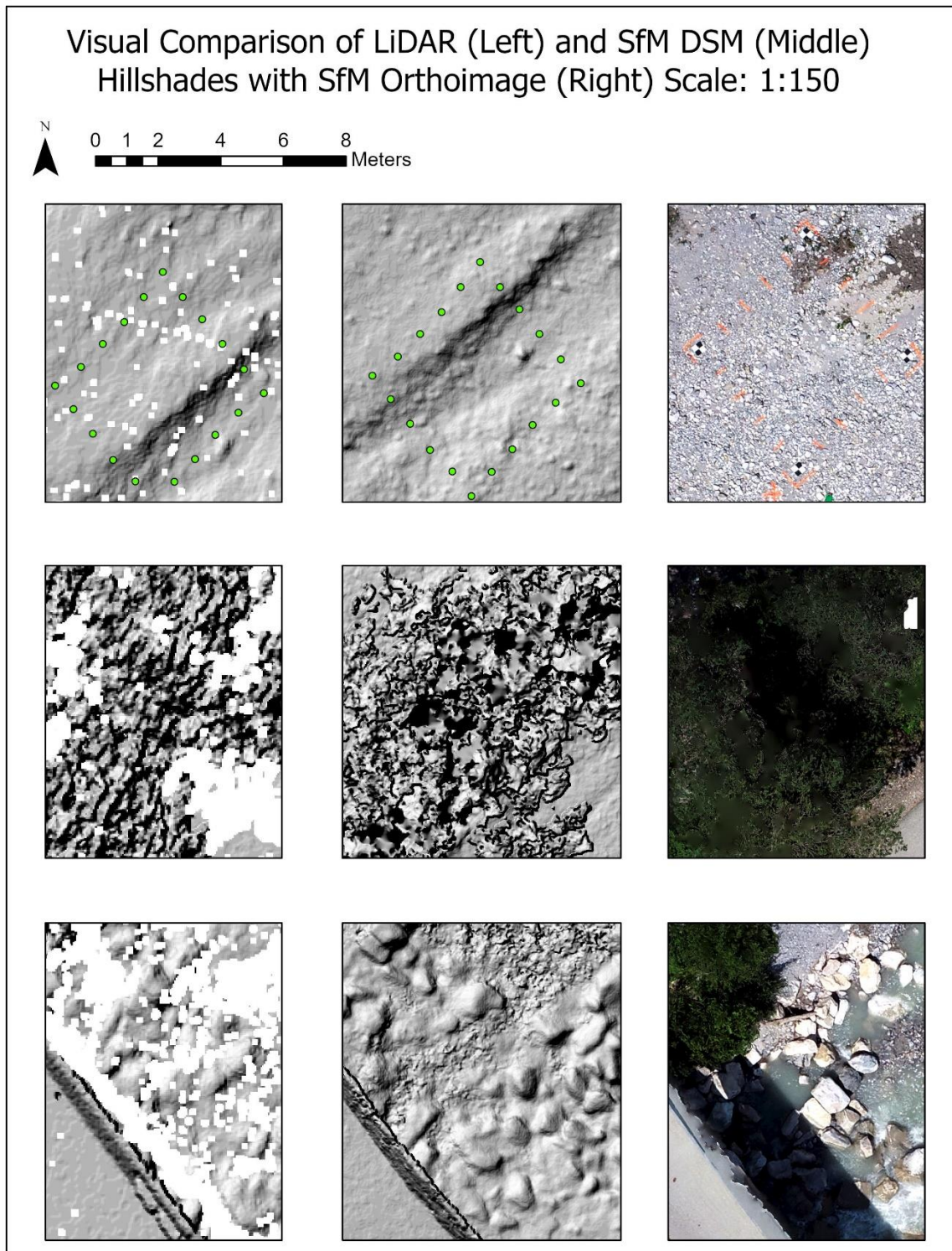


Figure 9 – A visual comparison of up close views of the orthoimage and hillshades produced using the LiDAR & SfM DSMs. The top row shows the study subplot. GNSS points were included in green to make the location clearer in the hillshades. The middle row is the top of a tree and the bottom row depicts an area in the creek with larger rocks, which would be somewhat analogous to the rocky intertidal.

Rugosity Comparison

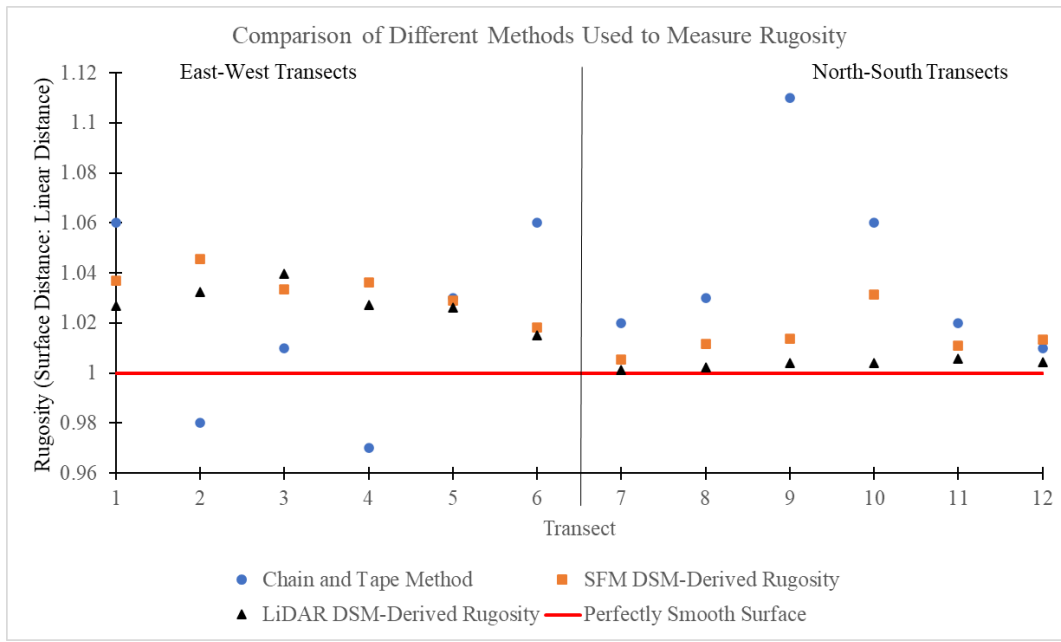


Figure 10- A comparison of rugosity measured in the field against the digitally derived rugosity measurements from the DSM. Rugosity is unitless.

The overall range of rugosity values from SfM, LiDAR, and the chain and tape method is 0.16. The small range shows that the subplot is relatively smooth and homogenous, and that all three methods generally agree. The SfM- and LiDAR-derived rugosity values closely agree whereas the chain and tape method shows more scattered values, an indication of more “noise” in the data (Figure 10). Like Figure 10, Figure 11 shows a small range of rugosity values, and with an R² value of 0.17, there is no apparent trend between plot size and rugosity, further supporting that the area is homogenous with subtle texture.

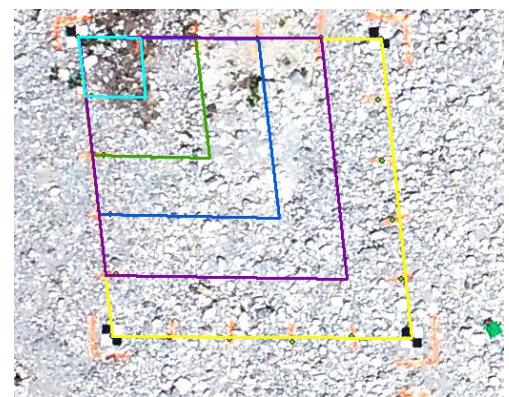
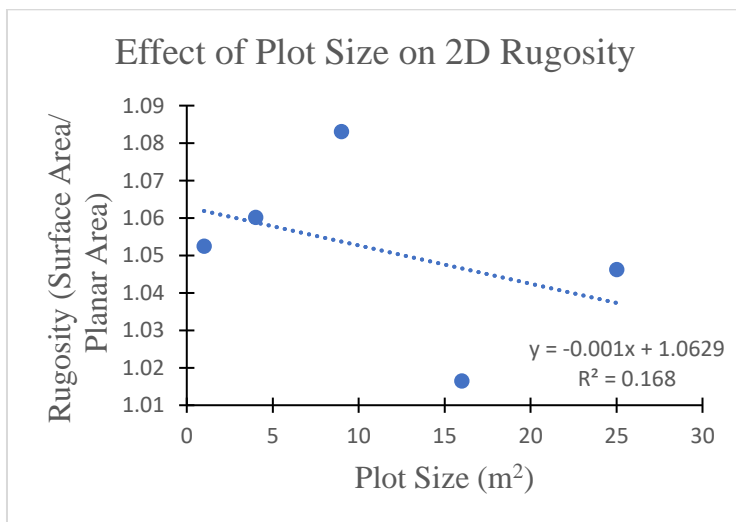
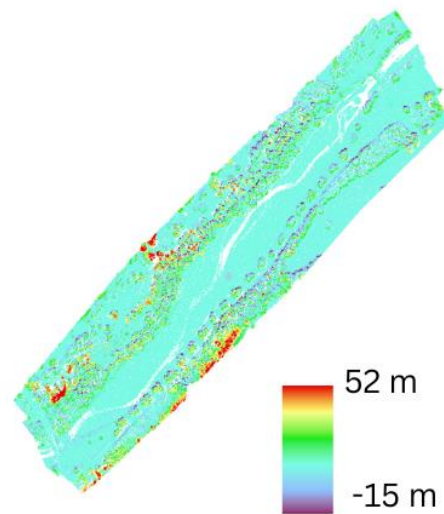
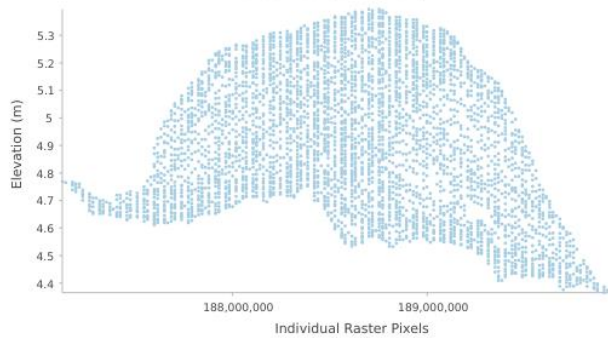


Figure 11 & 12- A scatterplot showing two-dimensional rugosity measurements (surface area: planar area) for various plot sizes within the 5 m x 5 m subplot, accompanied by an illustration of the different sized

Before Vertical Correction:

Difference Between LiDAR DSM and SfM DSM in Field Subplot Area (Prior to Vertical Correction)



After Vertical Correction:

Difference Between Vertically Corrected LiDAR DSM and SfM DSM in Field Subplot Area

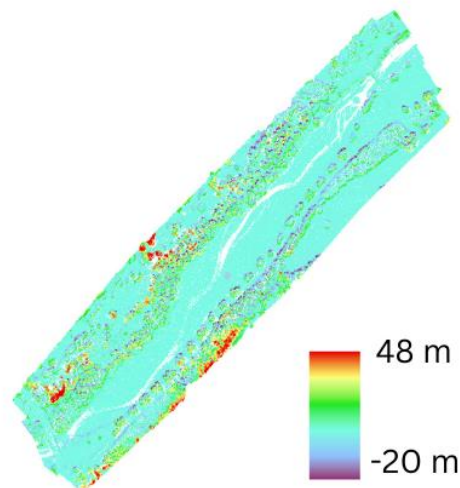
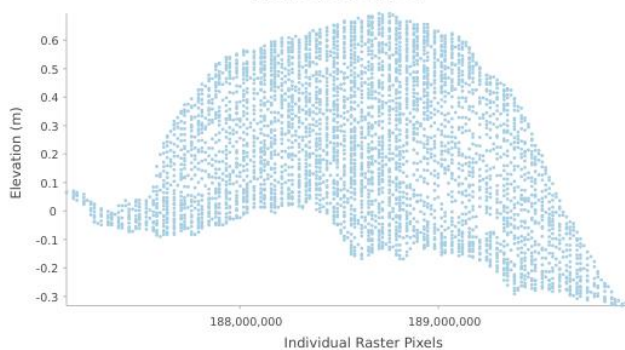


Figure 13 – An elevation raster created by subtracting the SfM DSM from the LiDAR DSM, before and after shifting the LiDAR DSM to account for the systemic error. The scatterplot shown is for the transect subplot area.

The DSMs had vertical height differences of 4 to 5 m in unvegetated areas, which was reduced following correction, as shown by the scatterplots (Figure 13). The patterns in the difference raster and the shape of the data distribution in the scatterplots are unchanged. The features in the difference DSM such as the bridge, roadway, hillslopes, rocks, and vegetation are still crisply visible, showing that the two DSMs co-register well, and that the disagreement is generally along the vertical axis. If the DSMs aligned poorly, these features would be distorted or indistinguishable.

Discussion & Conclusion

The source of vertical error in the LiDAR dataset is unknown. It could have been introduced during the LiDAR data processing, but most likely stems from a difference in the unknown vertical coordinate system. Additionally, the data was delivered in different x-y coordinate systems. The ground control points and the SfM data were delivered in EPSG 31255, and the LiDAR data were delivered in EPSG 31258. The LiDAR data were reprojected into EPSG 31255 to match the horizontal coordinate system of the other data. This reprojection complicates identifying the original vertical datum, likely rendering the task impossible. Furthermore, the systemic correction was based on an average value, and while it improved agreement between the two DSMs, it does not totally account for error, so it is difficult to determine how much of the difference between DSMs was due to this unknown error as opposed to differences between LiDAR and SfM, or signal to noise ratio.

However, most of the disagreement was concentrated in vegetated areas, which is entirely expected. SfM photogrammetry only captures the surfaces of objects, whereas LiDAR sensors can get as many as five returns per pulse. The multiple returns capture the structure of the vegetation beneath, inherently introducing disagreement. Additionally, because SfM relies on differential parallax, it is more sensitive to foliage movement. The disagreement was also strongest in the areas around the edges, which is likely due to insufficient overlap.

Given the strong agreement between SfM- and LiDAR-derived rugosity values, it is suspected that much of the disagreement between the two datasets at the DSM level in non-vegetated areas is due to random noise or remainders of the systemic error as opposed to differences in how well each system resolves surface detail.

Rugosity is most extensively measured at reefs, which are highly variable in their texture and complexity, but typical rugosity values for reefs range from about 1.2 to 4.0 (Holmes, 2008). By comparison, the rugosity subplot here is almost smooth. Values from all three methods generally reflect this, but there is more spread in the chain and tape values, suggesting that UAS remote sensing methods are a better method for quantifying rugosity than the chain and tape field method. There was almost no difference in rugosity values between SfM and LiDAR. This makes sense, as there's some level of human judgement involved in draping the chain along the transect. However, both the chain and tape method and the DSM approach described here are subject to the limitations identified by Frost et al. (2005) in that it is an average value over a transect, which cannot distinguish the size, number, or shape of corrugations. At this time, it is not possible to draw conclusions on the point cloud comparison, but the difficulties were almost certainly due to the size of the datasets.

An alternative explanation for the agreement of the rugosity values is that the surface has subtle variations, and they were within the noise with each method. However, this seems unlikely as both UAS remote sensing approaches have a vertical accuracy of around 1.5 cm and are more consistent with each other and between transects than they are with the established field method. If the UAS systems were not able to resolve the texture, it would show as a smooth surface (plotting along the red line) or perhaps exhibit more variation, similar to the chain and tape data points.

In evaluating the strengths and weaknesses of each method, SfM really shines. The SfM point cloud was much denser, and it was easier to identify the ground control point targets in the SfM point cloud and orthoimage than the colorized LiDAR. Workflows for Agisoft Metashape are largely automated and easy to learn. Additionally, LiDAR has only recently become small enough to work with UAS systems and is prohibitively expensive compared to SfM photogrammetry, which is possible in some cases with consumer-grade digital cameras (Garza

2019). LiDAR has an advantage in heavily shadowed areas or areas with low contrast as it does not rely on imagery to capture 3-D structure.

In conclusion, results from this pilot study suggest that both UAS SfM and LiDAR produce similar DSMs as well as rugosity measurements that are at least as accurate and precise than the most established field method. This is consistent with Shaw et al. (2019), where researchers compared UAS imagery to UAS LiDAR and found that both techniques were suitable for beach monitoring though LiDAR was more accurate and consistent with ground control points. Interestingly, they compared two UAS SfM systems with UAS LiDAR and found that both SfM datasets had positive vertical bias of four to nine cm in comparison to the LiDAR data.

Future Work

LiDAR sensors have only become light enough to use with UAV platforms in the past few years, largely due to advancements with autonomous vehicles. As this technology becomes more available, work remains in improving workflows (particularly for LiDAR datasets and point cloud comparisons). Additionally, this technology shows great promise for reducing costs and improving efficiency in habitat mapping and monitoring efforts. High resolution UAS imagery and DSMs are of particular interest for monitoring changes to intertidal habitat availability and zonation due to sea level rise.

With this project, future work remains in further developing a workflow to compare the datasets at a point cloud level, and in applying these methods to actual rocky intertidal sites. As I continue to progress toward completing my thesis, I will collect and process UAS SfM and LiDAR data at my proposed research sites in California. As rocky intertidal sites generally have more pronounced geological features than those seen in the ground truth subplot used here, it will be interesting to see how well the two systems compare in their ability to resolve detail, surface roughness, and species richness/abundance. Pilot studies in San Diego indicate that sessile species can easily be seen with SfM photogrammetry at low altitudes, but that motile taxa are not seen. Likely because they are cryptic, especially during low tide, when the drone missions are performed. Motile taxa are also small, approaching the lower threshold of what is identifiable at the resolution of some preliminary imagery taken in La Jolla, California as part of a test study. Sessile organisms are small individually, but occur in patches with reasonable color and texture contrast from the rocky substrate.

I will defend my thesis proposal early Spring 2023 semester, collect UAS LiDAR and SfM data in January 2023 and begin analysis shortly after that. My thesis will involve refining and implementing the methods described here at three rocky intertidal habitats in Laguna Beach, California. Additionally, I would like to use these datasets to delineate intertidal zonation, classify substrate types (possibly with object-based image analysis) and compare any visible organisms to reference biological survey data from the Multi-Agency Rocky Intertidal Network (MARINE).

Acknowledgements

Thank you to the Marshall Plan Foundation, Carinthia University of Applied Sciences, and San Diego State University for the opportunity to participate in this exchange program. The UAS LiDAR mission and LiDAR data postprocessing was performed by Rudi Schneeberger (iC Viewcopter; <https://www.vcopter.net/>), which is gratefully acknowledged. Thank you to Dr. Paulus (CUAS), Dr. Stow (SDSU), and Dr. Loerch (SDSU) for guiding this project.

References

- Barry et al. (1995). Climate-related, long-term faunal changes in a California rocky intertidal community. *Science*, 267(5198), 672–675.
<https://doi.org/10.1126/science.267.5198.672>
- Böhning-Gaese, K., Caprano, T., Ewijk, K., & Veith, M. (2006). Range size: Disentangling current traits and phylogenetic and biogeographic factors. *The American Naturalist*, 167(4), 555–567. <https://doi.org/10.1086/501078>
- Brock, J. C., Clayton, T. D., Nayegandhi, A., & Wright, C. W. (2004). Lidar optical rugosity of coral reefs in Biscayne National Park, Florida. *Coral Reefs*, 23(1), 48–59.
<https://doi.org/10.1007/s00338-003-0365-7>
- Burns et al. (2015). Integrating structure-from-motion photogrammetry with geospatial software as a novel technique for quantifying three dimensional ecological characteristics of coral reefs. *PeerJ*, 3. <https://doi.org/10.7717/peerj.1077>
- Camus et al. (1999) Effects of substratum topography on species diversity and abundance in Chilean rocky intertidal communities. *Revista Chilena de Historia Natural*, 72, 377–388.
- Carlson, R. L., Shulman, M. J., & Ellis, J. C. (2006). Factors contributing to spatial heterogeneity in the abundance of the common periwinkle *littorina littorea* (L.). *Journal of Molluscan Studies*, 72(2), 149–156. <https://doi.org/10.1093/mollus/eyi059>
- Collins et al. (2013). Rock-dwelling lizards exhibit less sensitivity of sprint speed to increases in substrate rugosity. *Zoology*, 116(3), 151–158.
<https://doi.org/10.1016/j.zool.2013.01.001>
- Cavanaugh et al. (2019). Climate-driven regime shifts in a mangrove–salt marsh ecotone over the past 250 years. *Proceedings of the National Academy of Sciences*, 116(43), 21602–21608. doi:10.1073/pnas.1902181116
- Connell (1961). The influence of interspecific competition and other factors on the distribution of the barnacle *chthamalus stellatus*. *Ecology*, 42(4), 710–723.
<https://doi.org/10.2307/1933500>
- Crosby et al. (2016). Salt marsh persistence is threatened by predicted sea-level rise. *Estuarine, Coastal and Shelf Science*, 181, 93–99.
doi:10.1016/j.ecss.2016.08.018
- Davey, K. (2000, January 4). *Life on Australian Seashores*. Tidal zonation, Eastern Warm Temperate Zone. Retrieved November 2, 2022, from <http://www.mesa.edu.au/friends/seashores/ewtz.html>
- Dayton (1971). Competition, disturbance, and community organization: The provision and subsequent utilization of space in a rocky intertidal community. *Ecological Monographs*, 41(4), 351–389. <https://doi.org/10.2307/1948498>
- Doughty et al. (2021). Characterizing spatial variability in coastal wetland Biomass across multiple scales using UAS and satellite imagery. *Remote Sensing in Ecology and Conservation*. <https://doi.org/10.1002/rse2.198>
- Dustan P, Doherty O, Pardede S (2013) Digital Reef Rugosity Estimates Coral Reef Habitat Complexity. *PLoS ONE* 8(2): e57386. <https://doi.org/10.1371/journal.pone.0057386>

- Enwright et al. (2018). The impact of lidar elevation uncertainty on mapping intertidal habitats on barrier Islands. *Remote Sensing*, 10(1). <https://doi.org/10.3390/rs10010005>
- Findlay et al. (2009). Post-larval development of two intertidal barnacles at elevated CO₂ and temperature. *Marine Biology*. 2010;157:725–35.
- Frost, N.J., Burrows, M.T., Johnson, M.P., Hanley, M.E. and Hawkins, S.J. (2005) Measuring surface complexity in ecological studies. *Limnology and Oceanography: Methods*, 3 (Apr), 203-210.
- Garza (2019). Landscape ecology in the Rocky INTERTIDAL: Opportunities for ADVANCING discovery and innovation in Intertidal research. *Current Landscape Ecology Reports*, 4(3), 83–90. <https://doi.org/10.1007/s40823-019-00042-8>
- Goddard et al. Nudibranch range shifts associated with the 2014 warm anomaly in the Northeast Pacific. *Bull So Calif Acad Sci*. 2016;115(1):15-40.
- Gosselin, L. A., & Qian, P.-Y. (1996). Early post-settlement mortality of an intertidal barnacle: a critical period for survival. *Marine Ecology Progress Series*, 135(1/3), 69–75. <http://www.jstor.org/stable/24857015>
- Harley et al. (2006). The impacts of climate change in coastal marine systems. In *Ecology Letters* (Vol. 9, Issue 2, pp. 228–241). <https://doi.org/10.1111/j.1461-0248.2005.00871.x>
- Helmuth et al. (2006). Living on the Edge of Two Changing Worlds: Forecasting the Responses of Rocky Intertidal Ecosystems to Climate Change *Annual Review of Ecology, Evolution, and Systematics*, 37(1), 373-404. doi:10.1146/annurev.ecolsys.37.091305.110149
- Harley, C. D., Helmuth, B. S. (2003). Local- and regional-scale effects of wave exposure, thermal stress, and absolute versus effective shore level on patterns of intertidal zonation. *Limnology and Oceanography*, 48(4), 1498–1508. <https://doi.org/10.4319/lo.2003.48.4.1498>
- Holmes, G. (2008). Estimating three-dimensional surface areas on coral reefs. *Journal of Experimental Marine Biology and Ecology*, 365(1), 67–73. <https://doi.org/10.1016/j.jembe.2008.07.045>
- Jackson & McIlvenny (2011). Coastal squeeze on rocky shores in northern Scotland and some possible ecological impacts. *Journal of Experimental Marine Biology and Ecology*, 400(1-2), 314-321. doi:10.1016/j.jembe.2011.02.012
- Kaplanis et al. (2020). Future sea-level rise drives rocky intertidal habitat loss and benthic community change. *PeerJ*, 8. <https://doi.org/10.7717/peerj.9186>
- Kolzenburg et al. (2016). Rapid updating and improvement of Airborne LIDAR DEMs Through Ground-Based SfM 3-d modeling of volcanic features. *IEEE Transactions on Geoscience and Remote Sensing*, 54(11), 6687–6699. <https://doi.org/10.1109/tgrs.2016.2587798>
- Konar & Iken (2017). The use of unmanned aerial vehicle imagery in intertidal monitoring. *Deep Sea Research Part II: Topical Studies in Oceanography*, 147, 79–86. <https://doi.org/10.1016/j.dsr2.2017.04.010>
- Kunze et al. (2021). Multiple Driver Impacts on Rocky Intertidal Systems: The Need for an Integrated Approach. In *Frontiers in Marine Science* (Vol. 8). Frontiers Media S.A. <https://doi.org/10.3389/fmars.2021.667168>
- Lecours, V., Devillers, R., Schneider, D. C., Lucieer, V. L., Brown, C. J., & Edinger, E. N. (2015). Spatial scale and geographic context in benthic habitat mapping: Review and future directions. In *Marine Ecology Progress Series* (Vol. 535, pp. 259–284). Inter-Research. <https://doi.org/10.3354/meps11378>

- Lin et al. (2019). Evaluation of UAS LIDAR for Mapping Coastal Environments. *Remote Sensing*, 11(24). <https://doi.org/10.3390/rs11242893>
- Meager et al. (2011). Topographic complexity and landscape temperature patterns create a dynamic habitat structure on a rocky intertidal shore. *Marine Ecology Progress Series*, 428, 1–12. <https://doi.org/10.3354/meps09124>
- MacArthur RH, MacArthur JW (1961) On bird species diversity. *Ecology* 42: 594–498.
- Menge et al. (2008). Response of a rocky intertidal ecosystem engineer and community dominant to climate change. *Ecology Letters*, 11(2), 151–162. <https://doi.org/10.1111/j.1461-0248.2007.01135.x>
- Menge & Menge (2013). CONCEPTS & SYNTHESIS EMPHASIZING NEW IDEAS TO STIMULATE RESEARCH IN ECOLOGY Dynamics of coastal meta-ecosystems: the intermittent upwelling hypothesis and a test in rocky intertidal regions. In *Ecological Monographs* (Vol. 83, Issue 3). <http://www.lme.noaa.gov>
- Mieszkowska et al. (2019). Multinational, integrated approaches to forecasting and managing the impacts of climate change on intertidal species. In *Marine Ecology Progress Series* (Vol. 613, pp. 247–252). Inter-Research. <https://doi.org/10.3354/meps12902>
- A. Nafidi, M. Bahij, B. Achchab, R. Gutiérrez-Sanchez (2019). The stochastic Weibull diffusion process: Computational aspects and simulation. *Applied Mathematics and Computation*, 348. DOI:10.1016/j.amc.2018.12.017.
- Nasrolahi et al. (2016). Temperature and salinity interactively impact early juvenile development: a bottleneck in barnacle ontogeny. *Marine Biology*. 2013;160(5):1109-17. doi: 10.1007/s00227-012-2162-8.
- Nex, F., & Remondino, F. (2013). UAV for three dimensional Mapping Applications: A Review. *Applied Geomatics*, 6(1), 1–15. <https://doi.org/10.1007/s12518-013-0120-x>
- Oppenheimer et al. 2019: Sea Level Rise and Implications for Low-Lying Islands, Coasts and Communities. In: *IPCC Special Report on the Ocean and Cryosphere in a Changing Climate* [H.-O. Pörtner, D.C. Roberts, V. Masson-Delmotte, P. Zhai, M. Tignor, E. Poloczanska, K. Mintenbeck, A. Alegría, M. Nicolai, A. Okem, J. Petzold, B. Rama, N.M. Weyer (eds.)].
- Paine (1966). Food web complexity and species diversity. *The American Naturalist*, 100(910), 65–75. <https://doi.org/10.1086/282400>
- Paine, R. T. (1966). Food web complexity and species diversity. *The American Naturalist*, 100(910), 65–75. <https://doi.org/10.1086/282400>
- Sarty et al. (2006). Habitat complexity facilitates coexistence in a tropical ant community. *Oecologia*, 149(3), 465–473. <https://doi.org/10.1007/s00442-006-0453-9>
- Schaefer et al. (2020). Predicting the impact of sea-level rise on intertidal rocky shores with remote sensing. *Journal of Environmental Management*, 261, 110203. doi:10.1016/j.jenvman.2020.110203
- Schiel et al. (2004). Ten years of induced ocean warming causes comprehensive changes in marine benthic communities. *Ecology*, 85(7), 1833-1839. doi:10.1890/03-3107
- Sedano et al. (2020). Understanding the effects of coastal defence structures on Marine biota: The role of substrate composition and roughness in structuring sessile, macro- and Meiofaunal Communities. *Marine Pollution Bulletin*, 157. <https://doi.org/10.1016/j.marpolbul.2020.111334>
- Sweet, W.V., R.E. Kopp, C.P. Weaver, J. Obeysekera, R.M. Horton, E.R. Thieler, and C. Zervas, 2017: *Global and Regional Sea Level Rise Scenarios for the United States*.

NOAA Technical Report NOS CO-OPS 083. NOAA/NOS Center for Operational Oceanographic Products and Services.

- Tait, L., Bind, J., Charan-Dixon, H., Hawes, I., Pirker, J., & Schiel, D. (2019). Unmanned Aerial Vehicles (UAVs) for Monitoring Macroalgal Biodiversity: Comparison of RGB and Multispectral Imaging Sensors for Biodiversity Assessments. *Remote Sensing*, *11*(19), 2332. MDPI AG. Retrieved from <http://dx.doi.org/10.3390/rs11192332>
- Thorner et al. (2014). Impacts of Climate-Change-Driven Sea Level Rise on Intertidal Rocky Reef Habitats Will Be Variable and Site Specific. *PLOS ONE*, *9*(1). doi:10.1371/journal.pone.0086130
- Tomanek, L., & Helmuth, B. (2002). Physiological ecology of rocky intertidal organisms: A synergy of concepts. *Integrative and Comparative Biology*, *42*(4), 771–775. <https://doi.org/10.1093/icb/42.4.771>
- Torio & Chmura (2013). Assessing Coastal Squeeze of Tidal Wetlands. *Journal of Coastal Research*, *290*, 1049-1061. doi:10.2112/jcoastres-d-12-00162.1
- Underwood (2000). Experimental ecology of rocky intertidal habitats: What are we learning? *Journal of Experimental Marine Biology and Ecology*, *250*(1-2), 51–76. [https://doi.org/10.1016/s0022-0981\(00\)00179-9](https://doi.org/10.1016/s0022-0981(00)00179-9)
- Walbridge et al. (2018). Unified geomorphological analysis workflows with benthic terrain modeler. *Geosciences*, *8*(3), 94. <https://doi.org/10.3390/geosciences8030094>
- Walker et al. (2009). Relationship of reef fish assemblages and topographic complexity on southeastern Florida coral reef habitats. *Journal of Coastal Research*, *10053*, 39–48. <https://doi.org/10.2112/si53-005.1>
- Wang et al. (2019). Mapping height and aboveground biomass of mangrove forests on Hainan Island using UAS-LiDAR sampling. *Remote Sensing*, *11*(18). <https://doi.org/10.3390/rs11182156>
- Zhu et al. (2019). Integrating UAS optical imagery and LiDAR data for assessing the spatial relationship between mangrove and inundation across a subtropical estuarine wetland. *ISPRS Journal of Photogrammetry and Remote Sensing*, *149*, 146–156. <https://doi.org/10.1016/j.isprsjprs.2019.01.021>

Appendix

July 11 SfM mission Report

Processing Report - finalized, GCPs included

03 August 2022



Survey Data

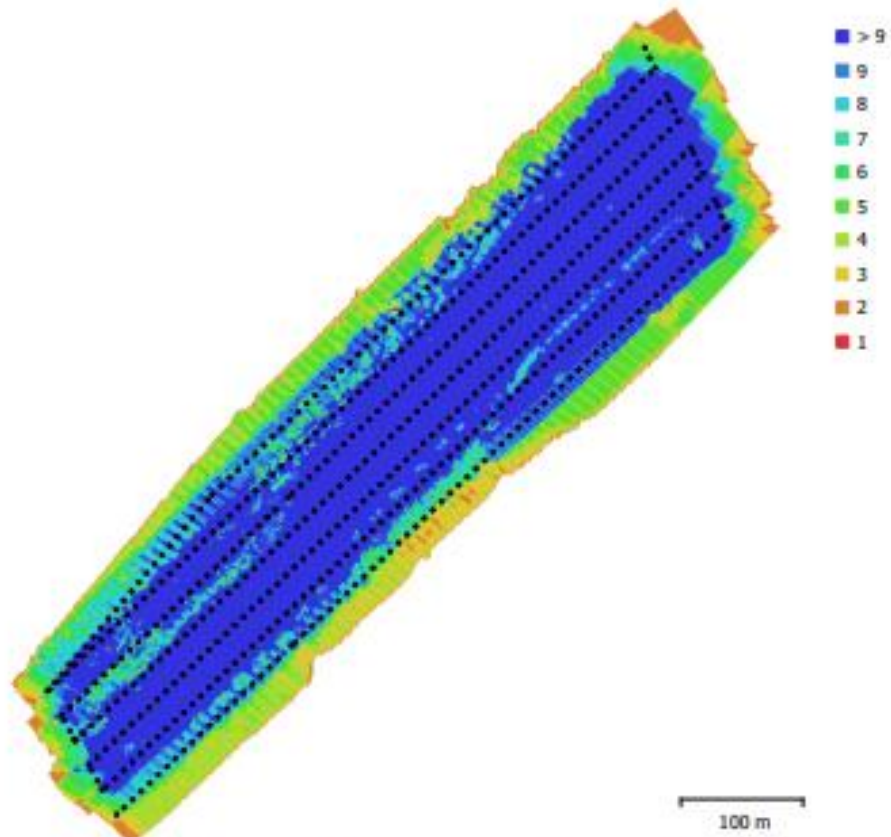


Fig. 1. Camera locations and image overlap.

Number of images:	528	Camera stations:	528
Flying altitude:	53.1 m	Tie points:	1,285,724
Ground resolution:	1.29 cm/pix	Projections:	5,083,745
Coverage area:	0.146 km ²	Reprojection error:	0.328 pix

Camera Model	Resolution	Focal Length	Pixel Size	Precalibrated
FC6310R (8.8mm)	5472 x 3648	8.8 mm	2.41 x 2.41 μ m	No

Table 1. Cameras.

Camera Calibration

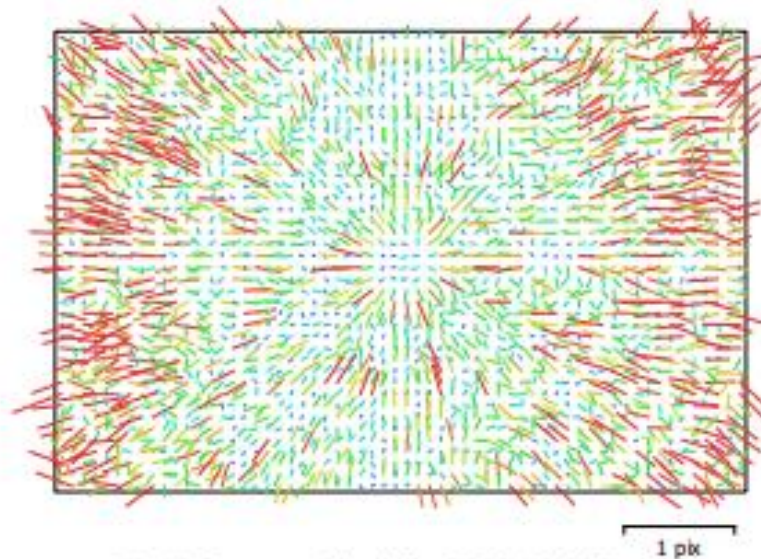


Fig. 2. Image residuals for FC6310R (8.8mm).

FC6310R (8.8mm)

528 images

Type	Resolution	Focal Length	Pixel Size
Frame	5472 x 3648	8.8 mm	2.41 x 2.41 μm

	Value	Error	F	Cx	Cy	B1	B2	K1	K2	K3	K4	P1	P2
F	3706.65	0.91	1.00	0.81	0.42	-0.07	-0.01	-0.25	-0.39	0.60	-0.66	-0.72	-0.71
Cx	-30.6376	0.029		1.00	0.36	-0.13	-0.03	-0.20	-0.32	0.49	-0.54	-0.50	-0.58
Cy	-11.5003	0.016			1.00	0.01	-0.10	-0.10	-0.17	0.25	-0.28	-0.32	-0.03
B1	0.306644	0.0044				1.00	0.07	0.03	0.01	-0.03	0.04	0.09	0.06
B2	0.227384	0.0045					1.00	-0.00	0.01	-0.01	0.01	0.01	0.00
K1	-0.00685059	1.4e-005						1.00	-0.72	0.52	-0.43	0.21	0.18
K2	-0.0290111	7.2e-005							1.00	-0.96	0.92	0.28	0.28
K3	0.0669159	0.00016								1.00	-0.99	-0.43	-0.43
K4	-0.0393673	0.00012									1.00	0.47	0.47
P1	-0.00199484	7.4e-007										1.00	0.49
P2	-0.00178367	6.6e-007											1.00

Table 2. Calibration coefficients and correlation matrix.

Ground Control Points



Fig. 3. GCP locations and error estimates.

Z error is represented by ellipse color. X,Y errors are represented by ellipse shape.
 Estimated GCP locations are marked with a dot or crossing.

Count	X error (cm)	Y error (cm)	Z error (cm)	XY error (cm)	Total (cm)
7	0.493375	0.351217	0.626213	0.605618	0.871157

Table 3. Control points RMSE.
 X - Easting, Y - Northing, Z - Altitude.

Count	X error (cm)	Y error (cm)	Z error (cm)	XY error (cm)	Total (cm)
4	0.895413	0.825505	2.05963	1.21788	2.39276

Table 4. Check points RMSE.
 X - Easting, Y - Northing, Z - Altitude.

Label	X error (cm)	Y error (cm)	Z error (cm)	Total (cm)	Image (pix)
1	-0.158083	0.028249	-0.121479	0.201358	0.903 (15)
2	-0.100475	-0.45548	0.785836	0.913836	0.539 (15)
3	0.58507	-0.430671	-0.716737	1.02054	0.747 (15)
4	-0.532149	0.673686	0.780312	1.16014	0.536 (15)
5	-0.485484	0.0144291	0.124433	0.501385	0.543 (18)
6	0.878872	0.110023	-0.979064	1.32026	0.584 (16)
7	-0.18775	0.059764	0.126699	0.234253	0.858 (19)
Total	0.493375	0.351217	0.626213	0.871157	0.691

Table 5. Control points.
X - Easting, Y - Northing, Z - Altitude.

Label	X error (cm)	Y error (cm)	Z error (cm)	Total (cm)	Image (pix)
8	0.860195	1.01631	-2.94206	3.22932	1.067 (16)
13	0.59705	0.810296	-1.62129	1.90831	1.027 (22)
18	-0.401774	0.652814	-1.0842	1.32781	0.994 (20)
23	-1.39615	0.781157	-2.12334	2.65857	0.719 (17)
Total	0.895413	0.825505	2.05963	2.39276	0.966

Table 6. Check points.
X - Easting, Y - Northing, Z - Altitude.

Digital Elevation Model

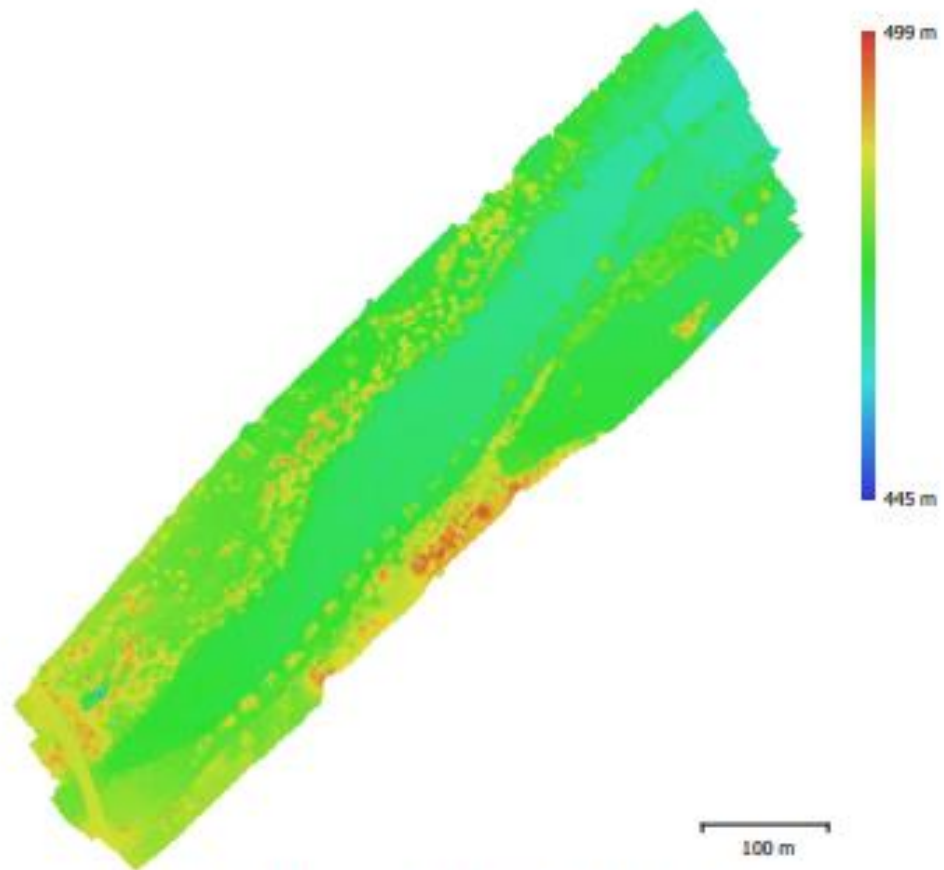


Fig. 4. Reconstructed digital elevation model.

Resolution: 2.58 cm/pix
Point density: 0.15 points/cm²

Processing Parameters

General

Cameras	528
Aligned cameras	528
Markers	11
Coordinate system	MGI / Austria GK Central (EPSG::31255)
Rotation angles	Yaw, Pitch, Roll

Point Cloud

Points	1,285,724 of 2,912,677
RMS reprojection error	0.198767 (0.327832 pix)
Max reprojection error	1.36158 (2.67326 pix)
Mean key point size	1.66599 pix
Point colors	3 bands, uint8
Key points	No
Average tie point multiplicity	3.07534

Alignment parameters

Accuracy	Highest
Generic preselection	Yes
Reference preselection	Yes
Key point limit	120,000
Tie point limit	0
Adaptive camera model fitting	No
Matching time	56 minutes 42 seconds
Alignment time	15 minutes 59 seconds

Optimization parameters

Parameters	f, b1, b2, cx, cy, k1-k4, p1, p2
Adaptive camera model fitting	No
Optimization time	21 seconds
Software version	1.5.5.9097

Depth Maps

Count	528
Depth maps generation parameters	
Quality	High
Filtering mode	Disabled
Processing time	7 hours 8 minutes
Software version	1.5.5.9097

Dense Point Cloud

Points	316,838,841
Point colors	3 bands, uint8

Depth maps generation parameters

Quality	High
Filtering mode	Disabled
Processing time	7 hours 8 minutes

Dense cloud generation parameters

Processing time	1 hours 7 minutes
Software version	1.5.5.9097

DEM

Size	32,477 x 33,999
Coordinate system	MGI / Austria GK Central (EPSG::31255)

Reconstruction parameters

Source data	Dense cloud
-------------	-------------

General

Interpolation	Enabled
Processing time	8 minutes 47 seconds
Software version	1.5.5.9097

Orthomosaic

Size	48,498 x 53,068
Coordinate system	MGI / Austria GK Central (EPSG::31255)
Colors	3 bands, uint8

Reconstruction parameters

Blending mode	Mosaic
Surface	DEM
Enable hole filling	Yes
Processing time	38 minutes 56 seconds
Software version	1.5.5.9097

Software

Version	1.5.5 build 9097
Platform	Windows 64